

# Photon-phonon parametric oscillation induced by the quadratic coupling in an optomechanical resonator

Lin Zhang,\* Fengzhou Ji, and Xu Zhang

*School of Physics and Information Technology, Shaanxi Normal University, Xi'an 710119, China*

Weiping Zhang

*Quantum Institute for Light and Atoms, Department of Physics,  
East China Normal University, No.500, Shanghai 200241, P. R. China*

A direct photon-phonon parametric effect of the quadratic coupling on the mean-field dynamics of an optomechanical resonator in the large-scale-movement regime is found and investigated. Under a weak pumping power, the mechanical resonator damps to steady state with a nonlinear static response sensitively modified by the quadratic coupling. When the driving power increases beyond the static energy balance, the steady states lose their stabilities via Hopf bifurcations and the resonator produces stable self-sustained oscillation (limit-circle behavior) with discrete energy of step-like amplitudes due to the parametric effect of the quadratic coupling, which can roughly be understood by the power balance of gain and loss on the resonator. A further increase of the pumping power can intrigue chaotic dynamic of the resonator via a typical routine of period-doubling bifurcation but which can be stabilized by the parametric effect through an inversion bifurcation process back to limit-circle states. The bifurcation-to-inverse-bifurcation transitions are numerically verified by the maximal Lyapunov exponents of the dynamics and which indicate an efficient way to suppress the chaotic behavior of the optomechanical resonator by the quadratic coupling. Furthermore, the parametric effect of the quadratic coupling on the dynamic transitions of an optomechanical resonator can be conveniently detected or traced by the output power spectrum of the cavity field.

PACS numbers: 42.50.Wk, 05.45.-a, 07.10.Cm, 42.50.Ct

## I. INTRODUCTION

In recent years, continuing interests on cavity optomechanical systems stimulate the study of light driven nanomechanical resonators in order to develop high-efficiency nano-motors, ultra-sensitive mass/force sensors or high-speed, low-energy consuming signal processors [1, 2]. In a red-detuned weak-driving regime, the quantum behaviors of nanomechanical resonators is the main topic of research, such as mechanical cooling, quantum state controlling, state engineering and state transferring, etc [3, 4]. However, under a strong, blue-detuned pumping field, a large-scale movement up to micrometers can be intrigued to evoke strong nonlinear properties of the nanomechanical resonators that invalidate the harmonic oscillator model. One of the important nonlinear effects emerged in this case is the quadratic coupling, a second order photon-phonon coupling in the optomechanical systems [5–10]. The nonlinear behavior with a large-amplitude of motion is dominated by the mean-field dynamics of the resonator and it is critical to explore new features of practical applications. One important nonlinear behavior found in the optomechanical systems is that the system can support stable self-sustained oscillations (SSOs) [11–14] and a high-efficiency broadband high-order harmonic oscillation can be generated in this

case [15, 16]. An easily controlled SSO working at different power levels is the physical foundation for many practical applications such as developing force sensors or information processors based on photon-phonon interactions [17]. Therefore, in this work, we will explore a photon-phonon parametric oscillation of the optomechanical resonator by considering its quadratic coupling in order to facilitate an adaptive application of this system in the future.

As the typical displacement of a nano-resonator is extremely small, the conventional optomechanical model considers only the linear photon-phonon coupling, whose magnitude is linearly proportional to the displacement of the mechanical resonator, and the quadratic coupling is very weak then. However, for a mechanical resonator in an extremely-large-amplitude regime [18], the weak quadratic coupling starts to play a non-ignorable role because its magnitude is proportional to the displacement squared. On the other hand, the chaotic behaviors of an optomechanical resonator in a red-detuned pumping field have been extensively verified in many optomechanical systems [19–23]. Recently, Bakemeier et. al. [21] studied the typical routes to chaos of a linear coupling optomechanical resonator in the weak pumping fields. They demonstrated a period-doubling bifurcation leading to chaos within a small displacement region which greatly limits the physical applications of optomechanical resonators due to the dynamical instabilities. Therefore, for a chaotic resonator, a very weak quadratic coupling will play a critical role to the nonlinear dynamics [24]. As

---

\*Electronic address: zhanglin.cn@snnu.edu.cn

have been shown in many optomechanical systems [5–10], the quadratic phonon-photon couplings bring manifest nonlinear properties even in a weak red-detuned pumping case and can lead to interesting parametric dynamics in a variety of optomechanical systems [25–29].

Based on the above discussions, we will closely consider the new dynamical features of a parametric optomechanical resonator induced by the quadratic couplings in this paper. We find a direct parametric effect of the quadratic coupling on the dynamical properties of the optomechanical resonator which is directly controlled by the intensity of the cavity field. The dynamic behavior modified by the parametric effect provide a solid way to stabilize the mechanical response of a nano-mechanical resonator, especially in the chaotic regions, and the nonlinear properties induced by the quadratic coupling can provide an easily controlled SSO with an enhanced sensitivity of its response to the external driving field in the critical parametric region. The combination of linear and quadratic coupling provides a tunable nonlinearity for the nano-resonators which can be further exploited to develop the reliable sensitive on-chip signal processors or the tunable mechanical sensors [27].

## II. THE PARAMETRIC EQUATION OF THE CROSS COUPLING RESONATOR

The Hamiltonian of an optomechanical oscillator with both linear and quadratic photon-phonon couplings can be written as [1, 15]

$$\hat{H} = \hat{H}_M + \hat{H}_{\text{cav}} + \hat{H}_{\text{pump}} + \hat{H}_\kappa + \hat{H}_\gamma, \quad (1)$$

where

$$\begin{aligned} \hat{H}_M &= \frac{\hat{p}^2}{2M} + \frac{1}{2}M\omega_M^2\hat{x}^2, \\ \hat{H}_{\text{cav}} &= -\hbar\delta_c\hat{a}^\dagger\hat{a} + \hbar G_1\hat{a}^\dagger\hat{a}\hat{x} + \frac{1}{2}\hbar G_2\hat{a}^\dagger\hat{a}\hat{x}^2 \\ \hat{H}_{\text{pump}} &= i\hbar[\eta(t)\hat{a}^\dagger - \eta^*(t)\hat{a}]. \end{aligned}$$

In the above model, the mechanical resonator  $\hat{H}_M$  with a free frequency of  $\omega_M$  couples with a cavity mode  $\hat{H}_{\text{cav}}$  of frequency  $\omega_c$  through a linear pressure coupling rate of  $G_1$  and a dispersive quadratic coupling rate of  $G_2$  [5]. The high-order quadratic coupling can be effectively derived from not only the nonlinear deformation of the cavity field but also the nonlinear properties of the mechanical resonators [8, 14, 30].  $\hat{H}_{\text{pump}}$  describes the cavity mode pumping by a classical field with a frequency of  $\omega_p$  and an amplitude of  $\eta$  related to its pumping power  $P$  by

$$P = |\eta|^2\hbar\omega_p/\kappa. \quad (2)$$

$\hat{H}_\kappa$  and  $\hat{H}_\gamma$  are the baths coupled to the cavity mode and the mechanical resonator and induce energy dissipations with the damping rates of  $\kappa$  and  $\gamma_M$ , respectively. The

pump-cavity detuning is defined by  $\delta_c = \omega_p - \omega_c$ , and the coupling rates of  $G_1$ ,  $G_2$  are given by  $G_1 = \omega'_c(x)$ ,  $G_2 = \omega''_c(x)$  for a linear cavity, where the prime means the spatial derivatives [1].

Based on the cross-coupling Hamiltonian of Eq.(1), the Heisenberg equation of motion for the mechanical resonator leads to a parametric oscillator described by

$$\frac{d^2\hat{x}}{dt^2} + \frac{\gamma_M}{2}\frac{d\hat{x}}{dt} + \omega_M^2\left(1 + \frac{\hbar G_2}{M\omega_M^2}\hat{a}^\dagger\hat{a}\right)\hat{x} = -\frac{\hbar G_1}{M}\hat{a}^\dagger\hat{a} + \frac{\hat{\xi}(t)}{M}, \quad (3)$$

where  $\hat{\xi}(t)$  accounts for the Langevin noise of the mechanical resonator. Clearly, Eq.(3) indicates that the quadratic coupling induces a direct parametric modification of the frequency of the resonator which consistently controlled by the cavity field intensity of  $\hat{a}^\dagger\hat{a}$ . For a conventional system with  $G_2 = 0$ , Eq.(3) reduces to

$$\frac{d^2\hat{x}}{dt^2} + \frac{\gamma_M}{2}\frac{d\hat{x}}{dt} + \omega_M^2\hat{x} = -\frac{\hbar G_1}{M}\hat{a}^\dagger\hat{a} + \frac{\hat{\xi}(t)}{M},$$

which only includes a pressure force induced by the cavity field through the linear coupling of  $G_1$ . Therefore, the quadratic coupling  $G_2$  in the above equation introduces further a parametric effect on the frequency of the resonator directly related to the intensity of the cavity field. The intensity of the cavity mode is then determined by

$$\frac{d}{dt}\hat{a}^\dagger\hat{a} = \eta\hat{a}^\dagger + \eta^*\hat{a} - \kappa\hat{a}^\dagger\hat{a} + \sqrt{\kappa}\left(\hat{a}^\dagger\hat{a}_{in} + \hat{a}_{in}^\dagger\hat{a}\right),$$

where  $\hat{a}_{in}$  describes the input noise of the light mode. Therefore, the optomechanical resonator with both linear and quadratic couplings results in a field-driven parametric oscillator [31–33] with field-dependent frequency and driving force. Although the quadratic coupling is weak, its parametric effect on the mechanical oscillation will definitely bring new dynamic features which would become manifest when the amplitude of the motion grows large and the intensity of the cavity field grows stronger. In this case, the mean-field motion will dominate the dynamics by masking all the quantum correlations of the system. Therefore the behavior of the resonator can be investigated by the mean values of the quantum operators in the sense of  $c$  numbers, such as  $\hat{x} \rightarrow \langle\hat{x}\rangle = x_c$ ,  $\hat{p} \rightarrow \langle\hat{p}\rangle = p_c$ ,  $\hat{a} \rightarrow \langle\hat{a}\rangle = a_c$  without considering any quantum fluctuations and correlations [34]. Therefore the dynamics of the system is governed by the following system of equations:

$$\begin{aligned} \frac{dx(\tau)}{d\tau} &= p(\tau), \\ \frac{dp(\tau)}{d\tau} &= -\frac{\gamma_M}{2}p - \Omega_c^2(\tau)x(\tau) - 2g_1I(\tau) \\ \frac{dX(\tau)}{d\tau} &= -[\delta_c - g_1x(\tau) - g_2x^2(\tau)]Y(\tau) \\ &\quad - \frac{\kappa}{2}X(\tau) + \eta(\tau), \\ \frac{dY(\tau)}{d\tau} &= [\delta_c - g_1x(\tau) - g_2x^2(\tau)]X(\tau) - \frac{\kappa}{2}Y(\tau), \end{aligned} \quad (4)$$

where  $x(\tau) = x_c/x_{zpf}$  and  $p(\tau) = p_c/p_{zpf}$  are the position and the momentum of the mechanical resonator scaled by  $x_{zpf} = \sqrt{\hbar/2M\omega_M}$  and  $p_{zpf} = \sqrt{\hbar M\omega_M/2}$ , respectively. The two field quadratures  $X(\tau)$  and  $Y(\tau)$  are defined by  $X(\tau) = (a_c + a_c^*)/2$  and  $Y(\tau) = -i(a_c - a_c^*)/2$  with the field intensity being  $I(\tau) = X^2(\tau) + Y^2(\tau)$  and the field-modulated frequency of the mechanical resonator is defined by  $\Omega_c(\tau) = \sqrt{1 + 4g_2 I(\tau)}$ . Particularly, the scaled linear and quadratic coupling rates are

$$g_1 = G_1 x_{zpf}/\omega_M, g_2 = \frac{1}{2} G_2 x_{zpf}^2/\omega_M, \quad (5)$$

respectively, and all the other parameters  $\delta_c, \gamma_M, \kappa$  are scaled by  $\omega_M$  for convenience with a scaled time of  $\tau = \omega_M t$ . In the above equations, the mean-time influence of the equilibrium bahts  $\hat{H}_\kappa$  and  $\hat{H}_\gamma$  are supposed to be zero for  $\langle a_{in}(\tau) \rangle = 0$  and  $\langle \xi(\tau) \rangle = 0$  in a classical time limit. The amplitude of the classical pumping field is supposed to be a real function of  $\eta(\tau)$  and also scaled by  $\omega_M$ .

Then the classical version of Eq.(3) becomes

$$\ddot{x}(\tau) + \frac{\gamma_M}{2} \dot{x}(\tau) + \Omega_c^2(\tau) x(\tau) = -2g_1 I(\tau). \quad (6)$$

Surely, Eq.(6) presents a typical parametric equation which enables a parametric driving of the resonator by the cavity field through the quadratic coupling, and, reversely, the motion of the mechanical resonator also provides a parametric modification on the cavity field's frequency. The quadratic coupling here converts a conventional resonator into a direct parametric oscillator and can bring new dynamic features of the system such as parametric amplification, resonance and stabilization. Uniquely, in the present case, the parametric effects are consistently controlled by the cavity field which also simultaneously produces a light pressure force on the resonator. Specifically, if the cavity field adaptively locks into a periodic motion, Eq.(6) will be a periodically driven parametric oscillator and the Floquet's theorem or the properties of Mathieu equation can reveal a rich dynamical behaviors of the optomechanical resonator. As Eq.(4) generally describes a parametric oscillator with a field-controlled frequency through the quadratic coupling, a slight modification on the quadratic coupling rate can surely influence the parametric process of the resonator by a consistent cavity field. In the following analysis we will adopt the parameters that are closely relevant to the experimental results and has been analyzed in detail in Ref.[7, 15].

### III. PARAMETRIC EFFECT ON STATIC RESPONSES

In a weak pumping field, the optomechanical resonator surely settles down to a steady state due to the dominate role of energy damping. The static response of the res-

onator is then determined by the steady state of [35]

$$x_s = -\frac{2g_1 I_s}{1 + 4g_2 I_s}, \quad (7)$$

$$I_s = \frac{\eta^2}{(\kappa/2)^2 + (\delta_c - g_1 x_s - g_2 x_s^2)^2}, \quad (8)$$

where  $I_s \equiv X_s^2 + Y_s^2$  is the steady intensity of the cavity field and  $\eta^2$  is the scaled input pumping power (see Eq.(2)). Then the static displacement responses of the resonator are determined by a quintic equation of

$$(\delta_c - g_1 x_s - g_2 x_s^2)^2 x_s + (\kappa/2)^2 x_s + 2\eta^2 (g_1 + 2g_2 x_s) = 0. \quad (9)$$

Eq.(9) reveals a clear nonlinear response of the resonator to the light field [36, 37] and its analytical solutions are impossible to obtain. As the quadratic coupling is very weak for  $g_2 \ll 1$ , Eq.(9) can be simplified to a quartic equation

$$a_4 x_s^4 + a_3 x_s^3 + a_2 x_s^2 + a_1 x_s + a_0 = 0, \quad (10)$$

where the coefficients are  $a_4 = 2g_1 g_2$ ,  $a_3 = g_1^2 - 2g_2 \delta_c$ ,  $a_2 = -2g_1 \delta_c$ ,  $a_1 = \delta_c^2 + (\kappa/2)^2 + 4g_2 \eta^2$ ,  $a_0 = 2g_1 \eta^2$ . Although the solutions of Eq.(10) are now available, an exact analysis on the static behaviors of  $x_s$  is still cumbersome. However, if both coupling rates  $|g_{1,2}| < 10^{-2}$ , the sign of discriminant of Eq.(10) is determined by  $-g_2 \delta_c$ , which implies that the number of real solutions of  $x_s$  is mainly controlled by the detuning  $\delta_c$  and the quadratic coupling  $g_2$  [35]. An exact numerical analysis on Eq.(9) is shown in Fig.1, which indicates that the static response of the resonator is very sensitive to the sign of quadratic coupling on a strong pumping amplitude [14]. Fig.1 reveals that the negative quadratic couplings enhance the nonlinear property of the mechanical resonator and the positive ones can remove the bistability response of the resonator to the pumping field. According to Eq.(7), the static displacement of the resonator approximately increases with the intensity of the cavity field due to the linear coupling  $g_1$ , i.e.  $\propto -g_1 I_s$ , and the extreme shift is determined only by the ratio of two coupling rates  $-g_1/2g_2$ . Although in most cases the quadratic coupling  $g_2$  is much smaller than the linear coupling  $g_1$ , it brings dramatic effects on the mechanical response if it meets a resonant case of  $g_2 \sim -1/4I_s$  demonstrated by the inset of Fig.1(a). Eq.(8), which is shown in Fig.1(c), reveals a double resonant peak of the intracavity intensity to the resonator's position and the splitting of a normal Lorentzian lineshape of the cavity field is  $\sqrt{g_1^2 + 4\delta_c g_2}/g_2$ , which is highly sensitive to the quadratic coupling. Surely, the splitting peak provides a reliable method to detect the quadratic coupling rate of an optomechanical resonator in the large-scale displacement regime.

The static responses modified by the quadratic coupling can be completely understood by an adiabatic potential generated by the cavity mode when the field oscillation is much faster than the motion of the mechanical

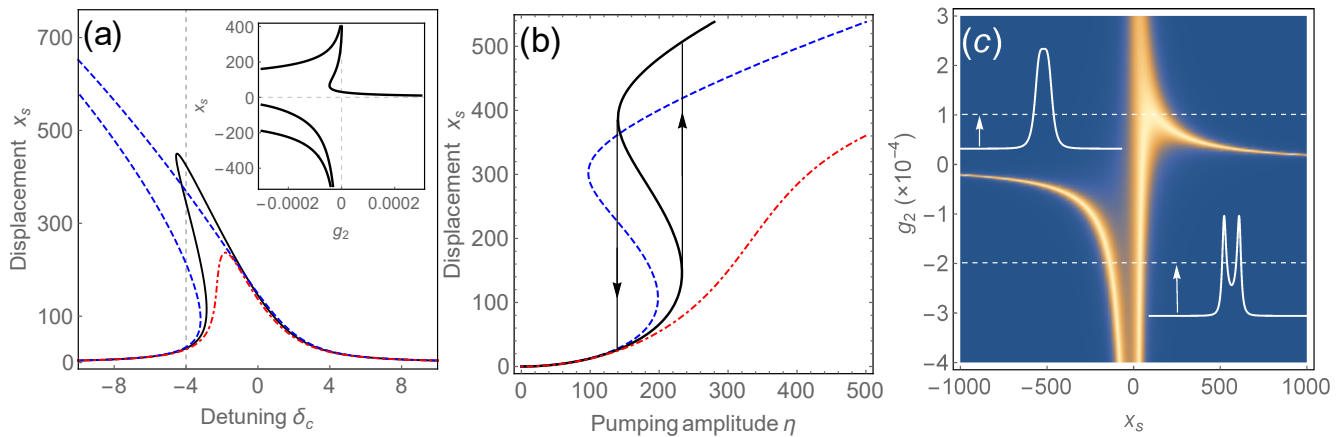


FIG. 1: (a) Quadratic modification on static displacement  $x_s$  versus pump detuning  $\delta_c$  with a fixed pumping power (amplitude  $\eta = 150$ ). Inset:  $x_s$  changes with the quadratic coupling under  $\delta_c = -4$ ; (b) The bistability responses of  $x_s$  to pumping amplitude  $\eta$  with a fixed detuning of  $\delta_c = -4$ . In both (a) and (b), the linear coupling  $g_1 = -0.01$  and the quadratic couplings are  $g_2 = -10^{-5}$  (blue dashed lines),  $g_2 = 0$  (black solid lines),  $g_2 = +10^{-5}$  (dot-dashed lines), respectively; (c) The intensity response of the intracavity field,  $I_s(g_2, x_s)$ , to the position of the resonator  $x_s$  and the quadratic coupling  $g_2$ , where  $\delta_c = -1$  and  $g_1 = -0.02$ . For all the above cases, the damping rate of the cavity field is  $\kappa = 2$ .

resonator. Then the total adiabatic potential felt by the resonator is [15]

$$U(x, \tau) = \frac{1}{2}x^2 - \frac{4\eta^2(\tau)}{\kappa} \arctan\left[\frac{\Delta(x)}{\kappa/2}\right], \quad (11)$$

where the effective position-dependent detuning

$$\Delta(x) = \delta_c - g_1x - g_2x^2. \quad (12)$$

The light-dressed adiabatic potential,

$$U_L(x) \equiv -\frac{4\eta^2}{\kappa} \arctan\left[\frac{\Delta(x)}{\kappa/2}\right], \quad (13)$$

is an arctangent function which will exhibit distinct properties due to the quadratic coupling as shown in Fig.2 (where  $\eta = 2$  is only for a convenient display). The light-induced potential  $U_L(x)$  will heavily dress the harmonic potential especially under a large pumping power of  $\eta^2$ . Fig.2 indicates that a negative quadratic coupling can enhance the nonlinear properties by introducing multiple stability and the positive one can suppress the nonlinear properties by enhancing the trapping force of the harmonic potential.

As the nonlinear responses of the resonator are manifest in a red-detuned pumping region ( $\delta_c < 0$ ) as shown in Fig.1, in the following sections, we will focus on the nonlinear dynamics of the mechanical resonator with both linear and quadratic couplings mainly in a red-detuned region. As the system is not a conservative system without time reversibility [38], we only consider the dynamics starting with a zero initial conditions (ground state) from a control point of view.

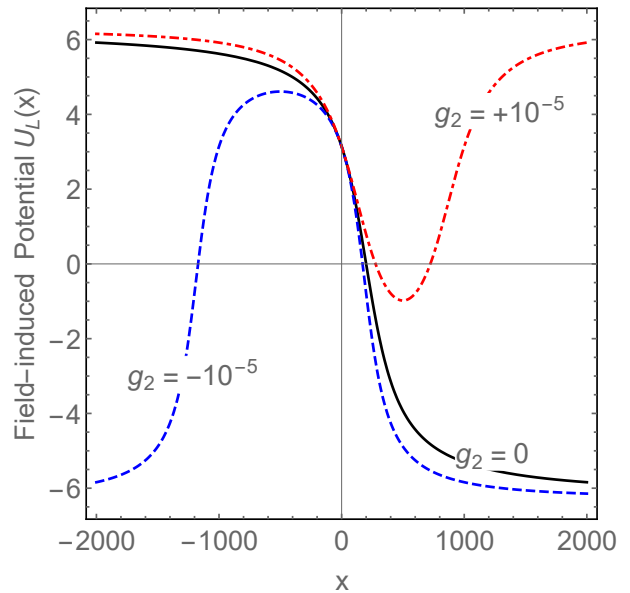


FIG. 2: The light-induced potential  $U_L(x)$  without (black solid line) and with negative (blue dashed line) and positive (red dot-dashed line) quadratic couplings. The other parameters are  $\eta = 2$ ,  $\delta_c = -2$ ,  $\kappa = 4$ ,  $g_1 = -0.01$ .

#### IV. PARAMETRIC AMPLIFICATION OF SSO WITH STEP-LIKE AMPLITUDES

The above nonlinear steady-state responses influenced by the quadratic coupling are based on the steady-state analysis without considering any dynamical stabilities of the system. However, when the pumping field is above a threshold power, the static behaviors shown in Fig.1 will lose their stabilities at a critical parametric point

and run into a limit-circle motion by a Hopf bifurcation [13–15], which is often identified as the SSO emerged in many nonlinear systems [17]. Fig.3 displays the typical

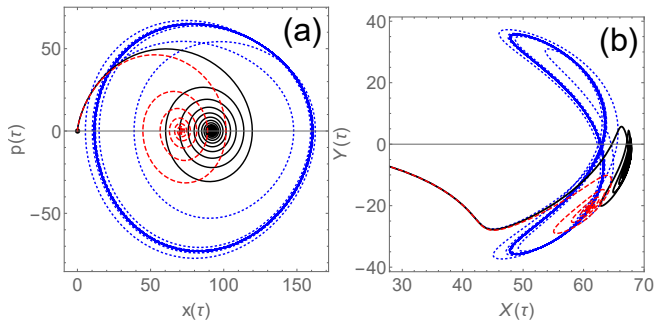


FIG. 3: (a) The dynamical trajectories of the mechanical resonator in the phase space and (b) the corresponding orbits of the two quadratures of the cavity field. The parameters are  $\gamma = 0.01, \kappa = 2, \delta_c = -1, \eta = 68, g_1 = -0.01$  and the quadratic couplings are  $g_2 = 0$  (solid black lines), and  $g_2 = -10^{-5}$  (dotted blue lines) and  $g_2 = 10^{-5}$  (dashed red lines), respectively.

dynamic orbits of the resonator and the corresponding cavity field in phase space starting from ground states in a red-detuned pumping field. We can see from Fig.3(a) that a very small negative quadratic coupling can sustain a self-oscillation (dotted blue line) in a parametric region where no SSO exists if only the linear coupling is included (solid black line). Fig.3(b) shows that this case corresponds a very typical parametric amplification process where the frequency of the cavity field (dotted blue line) is double the frequency of the resonator. However, a positive quadratic coupling will suppress the transition to the SSO under the same conditions (dashed red lines). When the resonator sustains a self-oscillation with a period time of  $T$  by the parametric amplification, its motion can be approximately described by

$$x(\tau) \approx x_0 + A \cos(\Omega\tau), \quad (14)$$

where  $x_0$  is the total displacement of the resonator mainly induced by the light pressure force,  $A$  is the average amplitude, and  $\Omega = 2\pi/T$  is the frequency of the SSO which can be estimated by a perturbation method around a small displacement as

$$\Omega \approx \sqrt{1 + \frac{4g_2\eta^2}{\left(\frac{\kappa}{2}\right)^2 + \delta_c^2} - \frac{\gamma_M^2}{16}}. \quad (15)$$

However, for a large-scale displacement, the above frequency will be invalid for the manifest nonlinear effect.

The resonator with a quadratic coupling can not only lock easily on SSO with a controllable amplitude, but also exhibits a very interesting limit-circle behavior compared with that of a conventional one. Fig.4 demonstrates that a weak negative quadratic coupling ( $g_2 = -10^{-5}$ ) can sustain stable SSOs with stair-like amplitudes (discrete energies) and a positive  $g_2$  can suppress the step jumping

behavior by a smooth increment with the same pumping power. The threshold power bursting into SSO shown in Fig.4(a) reveals that the negative quadratic coupling can generate SSO (the blue line) with a lower threshold than that does for a conventional one (the red line) in red-detuned pumping case, while, for the blue-detuned case shown in Fig.4(b), the bifurcation point remains the same with respect to the quadratic couplings but the amplitude of SSO is dramatically reduced. The energy bal-

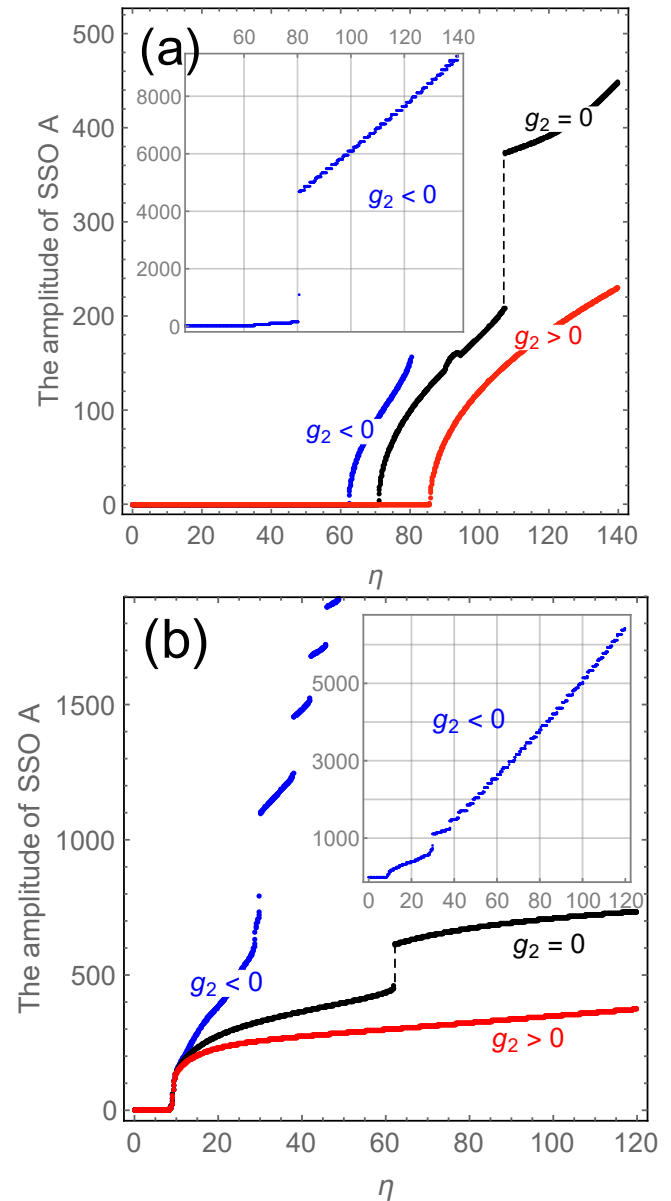


FIG. 4: The step-like amplitudes of SSO for (a) red-detuned case of  $\delta_c = -1$  and (b) blue-detuned case of  $\delta_c = 1$ . Insets: The full view of the amplitude stairs for (a) and (b). The other parameters are the same as that in Fig.3.

ance of loss and gain for the resonator can be used to determine the Hopf bifurcation point for a self-oscillation under different pumping powers. The parametric effect of

the quadratic coupling on the resonator's dynamic reveals that self-oscillation with discrete amplitudes can be easily controlled by the quadratic coupling, and the pumping power to sustain a stable self-oscillation is reduced by a negative quadratic coupling in the red-detuned pumping case as shown in Fig.4(a).

In order to understand the discrete amplitude of the self-oscillation, we can use the adiabatic equation for the resonator to give a rough analysis. When the resonator locks on a self-oscillation, the field intensity must also be periodic and the resonator approximately follows the adiabatic equation of

$$\ddot{x} + \frac{\gamma_M}{2}\dot{x} + (1 + 4g_2 I_c) x = -2g_1 I_c, \quad (16)$$

where the periodic cavity field  $I_c$  is

$$I_c(\tau) \approx \frac{\eta^2(\tau)}{\left(\frac{\kappa}{2}\right)^2 + \Delta^2(\tau)}.$$

As Eq.(16) should have a consistent solution with a form of Eq.(14), the motion-modulated detuning reads

$$\Delta(\tau) = A_0 + A_1 \cos \Omega t + 2A_2 \cos 2\Omega t,$$

where  $A_0 = (\delta_c - g_1 x_0 - g_2 x_0^2) - g_2 A^2/2$ ,  $A_1 = -A(g_1 + 2g_2 x_0)$ ,  $A_2 = -g_2 A^2/4$ . Now,  $I_c(\tau)$  is a periodic function of time and Eq.(16) becomes a damped and driven Mathieu equation which is stable for a solution of Eq.(14) only with the specific parameters. For a constant pumping power, the Floquet exponents of Eq.(16) can be used to analyze dynamical stability. A simple picture of the discrete amplitude shown in Fig.4 is that the adiabatic potential of Eq.(11) can induce an average multiple-well potential of

$$\bar{U}(A) = \frac{1}{T} \int_0^T U(x_0 + A \cos \Omega \tau, \tau) d\tau,$$

which supports the self-oscillation with step-like amplitudes with different  $x_0$  determined by the pumping power. A detailed analysis of the discrete amplitudes in this case should resort to the power balance of  $\langle \dot{x}\dot{x} \rangle = 0$  for the resonator [19], which gives [15]

$$A \approx \frac{8(g_1 + 2g_2 x_0) \bar{I}_1}{\Omega \gamma_M - 8g_2 \bar{I}_2}, \quad (17)$$

where  $\bar{I}_{1,2}$  are the average Fourier sine transforms of the cavity field (see Appendix A). Eq.(17) reveals that the amplitude of the self-oscillation can be increased or decreased by the quadratic coupling  $g_2$  in the denominator or in the numerator of Eq.(17) due to its parametric effect, and the resonant parametric amplification of SSO happens at  $\bar{I}_2 = \Omega \gamma_M / 8g_2$ . By using the long-time integral of Eq.(4) with Eq.(14), we have (see Appendix A)

$$\bar{I}_{1,2} \approx \eta^2 \times \text{Im} \left[ \sum_{n,m=-\infty}^{\infty} \sum_{n',m'=-\infty}^{\infty} \alpha_{n,m} \alpha_{n',m'}^* \right], \quad (18)$$

where  $\text{Im}[\cdot]$  means the imaginary part in the square brackets and the sums for  $\bar{I}_1$  and  $\bar{I}_2$  are taken under the resonant conditions of

$$n' - n + 2(m' - m) + 1 = 0,$$

and

$$n' - n + 2(m' - m) + 2 = 0,$$

respectively. The parameters  $\alpha_{n,m}$  are defined by [15]

$$\alpha_{n,m} = \frac{J_n(A_1) J_m(A_2)}{\frac{\kappa}{2} - i(A_0 + n\Omega + 2m\Omega)},$$

where  $J_n(\cdot)$  is the  $n$ -th order Bessel functions of the first kind. In Fig.5 we give a numerical calculation on the power structure of the resonator determined by

$$\bar{P}_m(x_0, A) = \frac{g_1 + 2g_2 x_0}{\Omega^2 A} \bar{I}_1 + \frac{g_2}{\Omega^2} \bar{I}_2 - \frac{\gamma_M}{8\Omega}.$$

We can see that the energy ‘‘gain’’ (the red area  $\bar{P}_m > 0$ ) and ‘‘loss’’ (the blue area  $\bar{P}_m < 0$ ) of the resonator depends on both mean displacement  $x_0$  and oscillation amplitude  $A$ , and the balanced curves of  $\bar{P}_m = 0$  for different pumping powers are shown by the white dashed lines in Fig.5. Basically, the light pressure of the cavity field ‘‘pushes’’ the resonator to give a total displacement which changes with the pumping power of  $\eta^2$  (see Fig.1(b)) and the amplitude of the resonator will modify itself along the white lines and conduct a jump between different white lines in order to follow the energy balance condition for different pumping powers. We can identify a clear change of the energy balance structure of the resonator that is sensitively modified by the quadratic coupling shifting from negative to positive. Fig.5 also indicates a localized gain region of the resonator (red area) due to the parametric stabilization effect introduced by the quadratic coupling.

## V. CHAOTIC DYNAMICS AND THE SUPPRESSION OF CHAOTIC BIFURCATIONS

However, in a pumping field with an even higher power, the regular self-oscillation will be unstable and the nonlinear resonator will break into chaos under some parametric conditions. A typical dynamic transition from a steady-state (the dashed line determined by Eq.(7)(8)) to chaotic dynamics is shown in Fig.6 by a jumping and a period-doubling bifurcation process. As shown in Fig.6, when the input energy from the pumping field exceeds the energy loss to the environments, the steady states of the resonator bursts into self-oscillations and then transit to chaotic oscillations via the typical period-doubling bifurcation routes [20, 21]. A complete dynamic behavior of a light-driven resonator shown in Fig.6 demonstrates three different transitions from steady state to SSO, to chaotic oscillation and finally back to SSO again along

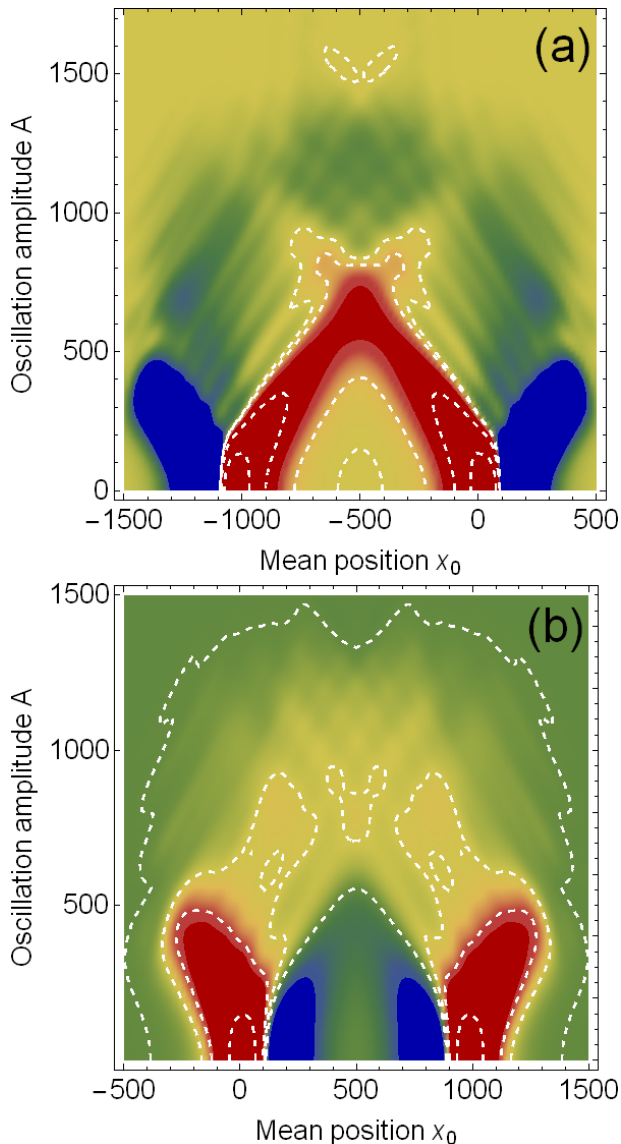


FIG. 5: The power balance structure of the resonator for (a) the negative quadratic coupling of  $g_2 = -10^{-5}$  and (b) the positive quadratic coupling of  $g_2 = 10^{-5}$  with a reference pumping amplitude of  $\eta = 100$ . The white dashed lines are the energy balanced curves calculated in different pumping power of  $\eta^2$ . The other parameters are  $\delta_c = -1$ ,  $\kappa = 2$ ,  $g_1 = -0.01$  and  $\Omega$  is determined by Eq.(15).

with the increasing power of the pumping field. The inset of Fig.6 displays the details of the period-doubling routes to chaos and the inverse bifurcations back to SSO with respect to the pumping power. We find a rich structure of the bifurcation-to-inverse-bifurcation window [19] embedded in the driving parametric region from  $\eta = 90$  to  $\eta = 101$  under the parameters shown in Fig.6.

Fig.7 picks several typical dynamical orbits of the resonator in the phase space to display one of the bifurcation-to-inverse-bifurcation window. At  $\eta = 90.7$  shown in Fig.7(a), the resonator takes an attractive

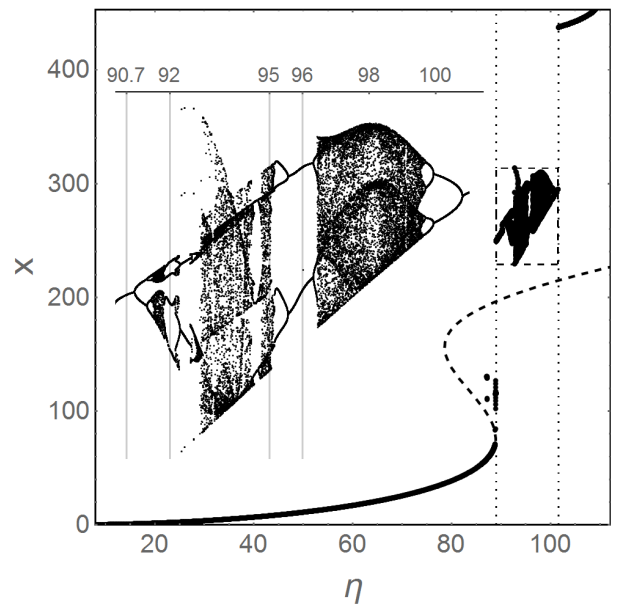


FIG. 6: A typical positive bifurcation structure of mechanical resonator's position versus pumping amplitude  $\eta$ . The parameters are  $\kappa = 2$ ,  $\gamma_M = 0.01$ ,  $\delta_c = -2$ ,  $g_1 = -0.01$  and  $g_2 = -10^{-5}$  with the zero initial conditions of  $x(0) = p(0) = X(0) = Y(0) = 0$ . The thick dashed line is the steady-state responsive curve. The inset gives the zoomed-in picture from the dashed rectangle.

period-1 orbit (a stable limit circle) and then breaks into a period-4 orbit at  $\eta = 92$  shown in Fig.7(b). One chaotic attractor is formed at  $\eta = 95$  shown in Fig.7(c) and then returns back to a 2-period orbit when the pumping amplitude increases to  $\eta = 96$  through an inverse bifurcation process.

We can identify this interesting chaotic dynamics by calculating the Lyapunov exponents (LEs) of the system as shown in Fig.8. We can clearly see that the maximal Lyapunov exponent (MLE) can be used to discriminate three different dynamics, the steady-state behavior with a negative MLE, the limit-circle motion with a zero MLE, and a positive MLE in the chaotic window along with abrupt droppings near to zero (inset of Fig.8). The very interesting thing is that the stability of the system is enhanced by a clear dropping of MLE at the critical pumping threshold around  $\eta = 89$ . This effect is due to the static “spring” effect of the light field [39, 40] which is proportional to  $\eta^2$  (see Eq.(13)) and can also be modified by the quadratic coupling. The zero value of MLE outside the chaotic window is a clear signature of the limit-circle dynamics of the resonator. For a motion on a limit circle, the LEs of the motion perpendicular to the orbit are negative but the LE along the trajectory is zero indicating a phase freedom of the limit-circle motion. This phase freedom along the orbit is the well-known mechanism leading to synchronization of a collection of resonators because the resonators can freely adjust their relative phases to achieve a synchronized motion [41].

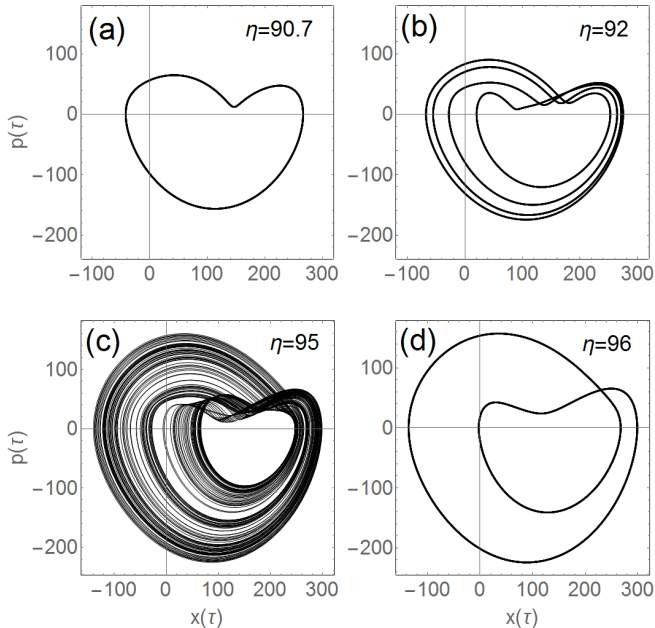


FIG. 7: The dynamic orbits of the mechanical resonator in the phase space for the specific pumping points at (a)  $\eta = 90.7$ , (b)  $\eta = 92$ , (c)  $\eta = 95$  and (d)  $\eta = 96$ , respectively. The other parameters are the same as that in Fig.6.

The chaotic dynamics of the mechanical resonator has been found extensively in the conventional optomechanical systems [19–23], but, in a system with both linear and quadratic couplings, the bifurcation and the inverse bifurcation with respect to light driving can be easily modified by a weak quadratic coupling. The sensitive modifications on chaotic transition in a nearly resolved sideband case ( $\kappa = \omega_M$ ) are shown in Fig.9. The different dynamics under different quadratic coupling rates clearly verify the parametric modulating effect of the dynamics on the mechanical resonator, which, totally, stabilizes the motion of the resonator (compare Fig.9(a)(c) with Fig.9(b)) [42]. In a weak pumping power, the mechanical resonator damps to steady state with a negative MLE due to the overwhelming energy dissipations and its nonlinear dynamics can be approximately explained by the adiabatic motion under potential of Eq.(11) [14]. With an increasing pumping power, the damping of the oscillation will be balanced and a stable SSO is established [15, 34], which is indicated by a zero MLE shown at the bottom frames of Fig.9. The interesting thing is that the resonator will adjust its position with a process of bifurcation and inverse bifurcation, and then follows by a jumping to a larger position with a new bifurcation. The MLE shown in Fig.8 indicates that there exist several bifurcation windows at different pumping powers and one of which is picked to show by the insets of Fig.9. When the pumping power becomes stronger, the mechanical resonator will lock itself to a stable oscillation governed by the light pressure of  $-2g_1I(\tau)$ . In this ex-

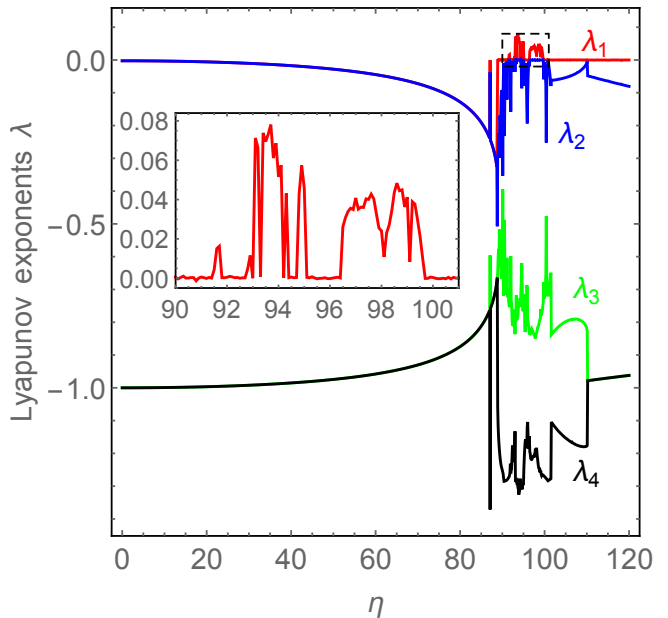


FIG. 8: The Lyapunov exponents  $\lambda_1, \lambda_2, \lambda_3$  and  $\lambda_4$  of the optomechanical system corresponding to Fig.6. The inset shows the zoomed-in image from the dashed rectangle of the maximal Lyapunov exponent  $\lambda_1$ . All the parameters are the same as that in Fig.6.

treme case, the resonator will be approximately treated as a forced resonator because the right term of Eq.(6) will dominate the resonator’s dynamics.

## VI. FIELD SIGNATURE OF DYNAMIC TRANSITIONS

As the intensity of the cavity field parametrically couples to the motion of mechanical resonator, the dynamical transition of the mechanical resonator can definitely influence the cavity field through a back-action effect. If we stabilize the pumping power of the driving field, then the longtime amplitude of the cavity field is given by (see Appendix A)

$$a_c(\tau) \approx \eta e^{-\frac{\kappa}{2}\tau + i\theta(\tau)} \int_0^\tau e^{\frac{\kappa}{2}t - i\theta(t)} dt, \quad (19)$$

where the field frequency of  $a_c(\tau)$  is now determined by the position-dependent integral of

$$\theta(\tau) = \delta'_c \tau - g_2 \int_0^\tau x'^2(t) dt, \quad (20)$$

where  $\delta'_c = \delta_c + g_1^2/4g_2$ ,  $x'(t) = x(t) + g_1/2g_2$ . Eq.(20) shows that the spectrum of the cavity field is closely related to the dynamical phase of  $\theta(\tau)$ , which depends on the energy of the resonator estimated by  $E(\tau) \propto x'^2(t)$ . Generally, for a regular motion, the resonator can be described by  $x(t) \approx x_0 + \sum_n A_n(t) \cos(\Omega_n t)$ , where  $A_n(t)$

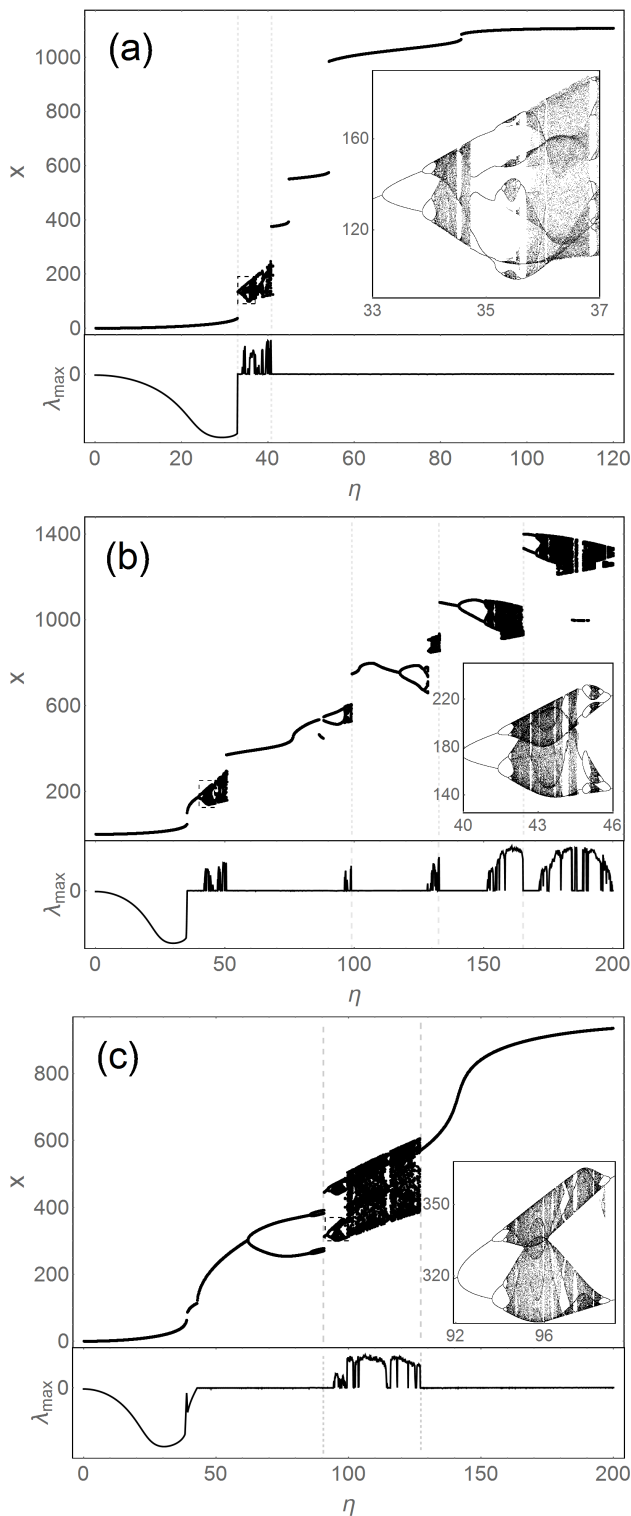


FIG. 9: Positive displacement bifurcations (top) and the corresponding maximal Lyapunov exponents (bottom) of the resonator vs pumping amplitude  $\eta$  modified by the quadratic couplings of (a)  $g_2 = -10^{-5}$ , (b)  $g_2 = 0$ , and (c)  $g_2 = 10^{-5}$ , respectively. The insets show the zoomed-in bifurcation images from the corresponding dashed rectangles. The other parameters are  $g_1 = -0.01$ ,  $\kappa = 1$ ,  $\gamma_M = 0.01$ ,  $\delta_c = -1$  with zero initial conditions.

is the instantaneous amplitude of the motion corresponding to the component of  $\Omega_n$ , but for a chaotic motion,  $A_n(t)$  will be a continuous function of  $A(\Omega, t)$ . Therefore, a close connection between the dynamics of resonator and the spectrum of the cavity field can be established by Eq.(19). Based on the input-output relation of the cavity field, the dynamic transition of the resonator can be readily detected from the output field of the cavity mode.

By investigating the power spectral density (PSD) of the cavity field, the motion of the mechanical resonator can be easily traced down. Fig.10(a)-(d) present four sample orbits of the mechanical resonator in the phase space with a negative quadratic coupling rate, and the corresponding power spectra of the cavity fields are displayed in the right column from (e) to (h). Fig.10 indicates a close connection of the mechanical dynamics with the power spectrum of the cavity field. In a relative low pumping power at  $\eta = 33$ , the resonator maintains its intrinsic frequency on a limit circle but has a very weak back action on the cavity field. The power spectrum of the cavity field exhibits a very weak side-band peak near the field-modulated frequency of  $\Omega$  (see Eq.(15)) and a relative stronger parametric peak near  $2\Omega$ . This spectral profile for a parametric amplification can be verified by the phase trajectory of the field quadratures,  $X$  and  $Y$ , shown by the inset of Fig.10(e). When the pumping amplitude increases to  $\eta = 34$ , the resonator steps into a period-doubling region and the power spectrum exhibits more resonant side-band peaks at harmonic and subharmonic frequencies around  $\omega_c \pm n\Omega/m$ , where  $n$  and  $m$  are integers. A chaotic dynamics (MLE is positive) at pumping amplitude of  $\eta = 40$  will induce a nearly continuous power spectrum for the cavity field as shown in Fig.10(g) [20]. When the pumping amplitude reaches  $\eta = 43$ , the mechanical resonator returns back to a limit-circle dynamics and the corresponding power spectrum displays a higher peak of the double frequency for an enhanced parametric amplification as shown in Fig.10(h) [19]. Therefore the power spectrum of the cavity field can be an indicator to trace the dynamical transitions of the mechanical resonator and then a feedback control on the dynamical transition of the mechanical resonator can be subsequently developed.

## VII. CONCLUSIONS AND DISCUSSION

By analyzing an optomechanical resonator with both linear and quadratic couplings, we give an explicit photon-phonon parametric model to find an interesting SSO with step-like amplitude and a tunable chaotic bifurcation to inverse bifurcation of the resonator based on the mean-field dynamics of Eq.(4) in a red-detuned pumping field. We investigate the parametric effects of the quadratic couplings to modify the dynamics of mechanical resonator and compare the different dynamical transitions between limit-circle oscillations and the chaotic dynamics. The static analysis reveals a very sensitive

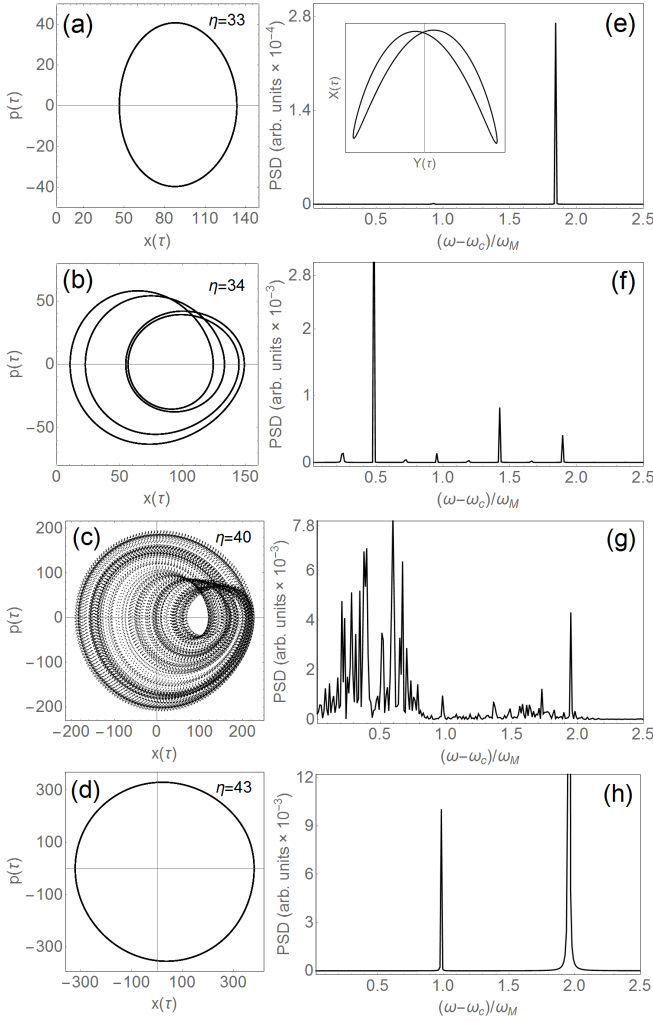


FIG. 10: The dynamical orbits of the mechanical oscillator in the phase space (the left column) and the corresponding power spectral density of the cavity fields (the right column). The dynamical parameters are  $\delta_c = -1$ ,  $\kappa = 1$ ,  $\gamma = 0.01$ ,  $g_1 = -0.01$  and  $g_2 = -10^{-5}$ .

quadratic effect on the position control of the mechanical resonator. The dynamical calculations give new features of the quadratic couplings and find interesting dynamical bifurcations of the mechanical resonator inducing different backactions on the field spectrum. Our study, firstly, shows that the optomechanical system with quadratic coupling provides a direct parametric process which can be actuated and controlled simultaneously by the intensity of the cavity field. This photon-phonon parametric system has advantages that its nonlinear behavior can be easily controlled by the pumping field and it can work in a red-detuned region with a low pumping power and thermal noise. The parametric effect found in this system gives a controllable oscillator to study the dynamical transitions, chaotic behaviors and the parametric process under a crossover from classical to quantum regime [24]. The study of classical squeezing [25, 31] verified by

the parametric effect also presents refined applications based on the nonlinearity of this system, such as to realize coherent frequency mixing and parametric coupling network of optomechanical systems with quadratic couplings. The classical dynamics shows the possibility of squeezing the resonator by quadratic coupling along with a cooling by the linear coupling simultaneously [25]. The dynamics of this system are much more richer than the conventional optomechanical system, and it can be easily detected by the power spectra of the field mode.

With both the quadratic and linear coupling, the quantum chaotic effects near the ground state will be an interesting topic on this model [23]. The quadratic coupling can generate non-classical states and give quantum nondemolition measurement on the energy of the nanomechanical resonator [43, 44]. In quantum regime, the strong cross-correlation between the light's and the resonator's motion will lead to new dynamical features beyond the mean-field dynamics. To explore these possibilities, a further work of nonlinear effect on full quantum dynamics should be done on this model.

### Acknowledgments

This work is supported by the National Natural Science Foundation of China (NSFC) Grant No.11447025, No.11234003 and the Scientific Research Foundation for the Returned Overseas Chinese Scholars, State Education Ministry.

### Appendix A: The spectrum of the cavity field

The amplitude of the cavity field is determined by

$$\frac{d}{d\tau} a_c(\tau) = \left[ i\Delta(x, \tau) - \frac{\kappa}{2} \right] a_c(\tau) + \eta(\tau), \quad (\text{A1})$$

and the formal solution is

$$a_c(\tau) = e^{-\frac{\kappa}{2}\tau} e^{i \int_0^\tau \Delta(x, t) dt} \times \left[ a(0) + \int_0^\tau e^{\frac{\kappa}{2}t} e^{-i \int_0^t \Delta(x, t') dt'} \eta(t) dt \right].$$

For a long time limit  $\tau \rightarrow \infty$ , the first term disappears, and then

$$a_c(\tau) \approx e^{-\frac{\kappa}{2}\tau + i\theta(\tau)} \int_0^\tau e^{\frac{\kappa}{2}t - i\theta(t)} \eta(t) dt, \quad (\text{A2})$$

where the dynamical phase integral is defined by

$$\theta(\tau) \equiv \int_0^\tau \Delta(x, t) dt.$$

If we put Eq.(14) into the above equation and set  $\eta(t) = \eta$  to be a constant pumping, we have

$$a_c(\tau) \approx \eta e^{(iA_0 - \frac{\kappa}{2})\tau} e^{iA_1 \sin(\Omega\tau)} e^{iA_2 \sin(2\Omega\tau)} \times \sum_{n, m=-\infty}^{\infty} J_n(A_1) J_m(A_2) F(\tau),$$

where  $e^{-iA \sin(\Omega t)} = \sum_{n=-\infty}^{\infty} J_n(A) e^{-in\Omega t}$  and

$$F(\tau) = \int_0^\tau e^{[\frac{\kappa}{2} - i(A_0 + n\Omega + 2m\Omega)]t} dt \\ = \frac{e^{[\frac{\kappa}{2} - i(A_0 + n\Omega + 2m\Omega)]\tau} - 1}{\frac{\kappa}{2} - i(A_0 + n\Omega + 2m\Omega)}.$$

Therefore, the long-time amplitude of the cavity field is

$$a_c(\tau) \approx \eta e^{iA_1 \sin(\Omega\tau)} e^{iA_2 \sin(2\Omega\tau)} \\ \times \sum_{n,m=-\infty}^{\infty} \frac{J_n(A_1) J_m(A_2)}{\frac{\kappa}{2} - i(A_0 + n\Omega + 2m\Omega)} e^{-i(n+2m)\Omega\tau},$$

and its intensity is

$$I(\tau) \approx \eta^2 \sum_{n,m;n',m'} \alpha_{n,m} \alpha_{n',m'}^* e^{i[(n'-n)+2(m'-m)]\Omega\tau}.$$

The time-average integrals of  $\bar{I}_1$  and  $\bar{I}_2$  are defined by

$$\bar{I}_1 \approx \langle I(\tau) \sin(\Omega\tau) \rangle = \text{Im} \left[ \frac{1}{T} \int_0^T I(\tau) e^{i\Omega\tau} d\tau \right], \\ \bar{I}_2 \approx \langle I(\tau) \sin(2\Omega\tau) \rangle = \text{Im} \left[ \frac{1}{T} \int_0^T I(\tau) e^{2i\Omega\tau} d\tau \right],$$

where  $T = 2\pi/\Omega$ . If we use the formula

$$\frac{\Omega}{2\pi} \int_0^{2\pi/\Omega} e^{i(n'-n)\Omega\tau} d\tau = \delta_{n,n'}, \quad (\text{A3})$$

we can obtain Eq.(18) with the corresponding sum rules.

- 
- [1] M. Aspelmeyer, T. J. Kippenberg, and F. Marquardt, *Cavity optomechanics*, Rev. Mod. Phys. **86**, 1391 (2014).
- [2] A. A. Clerk, M. H. Devoret, S. M. Girvin, F. Marquardt, and R. J. Schoelkopf. *Introduction to quantum noise, measurement, and amplification*, Rev. Mod. Phys. **82**, 1155 (2010).
- [3] M. Poot and H. S. J. vander Zant, *Mechanical systems in the quantum regime*, Phys. Rep. **511**, 273 (2012).
- [4] M. Aspelmeyer, P. Meystre and K. Schwab, *Quantum optomechanics*, Phys. Today **65**, 29 (2012).
- [5] J. D. Thompson, B. M. Zwickl, A. M. Jayich, F. Marquardt, S. M. Girvin and J. G. E. Harris, *Strong dispersive coupling of a high-finesse cavity to a micromechanical membrane*, Nature **452**, 72 (2008).
- [6] D. E. Chang, C. A. Regal, S. B. Pappb, D. J. Wilsonb, J. Ye, O. Painter, H. J. Kimbleb and P. Zoller, *Cavity optomechanics using an optically levitated nanosphere*, PNAS **107**, 1005 (2010).
- [7] J. C. Sankey, C. Yang, B. M. Zwickl, A. M. Jayich and J. G. E. Harris, *Strong and tunable nonlinear optomechanical coupling in a low-loss system*, Nature Physics **6**, 707 (2010).
- [8] V. Peano and M. Thorwart, *Macroscopic quantum effects in a strongly driven nanomechanical resonator*, Phys. Rev. B **70**, 235401 (2004).
- [9] T. P. Purdy, D. W. C. Brooks, T. Botter, N. Brahms, Z.-Y. Ma and D. M. Stamper-Kurn, *Tunable Cavity Optomechanics with Ultracold Atoms*, Phys. Rev. Lett. **105**, 133602 (2010).
- [10] S. Gupta, K. L. Moore, K. W. Murch and D. M. Stamper-Kurn, *Cavity Nonlinear Optics at Low Photon Numbers from Collective Atomic Motion*, Phys. Rev. Lett. **99**, 213601 (2007).
- [11] C. Metzger, M. Ludwig, C. Neuenhahn, A. Ortlieb, I. Favero, K. Karrai, F. Marquardt, *Self-Induced Oscillations in an Optomechanical System Driven by Bolometric Backaction*, Phys. Rev. Lett. **101**, 133903 (2008).
- [12] T. Carmon, H. Rokhsari, L. Yang, T. J. Kippenberg and K. J. Vahala, *Temporal behavior of radiation-pressure-induced vibrations of an optical microcavity phonon mode*, Phys. Rev. Lett. **94**, 223902 (2005).
- [13] H. Okamoto, D. Ito, K. Onomitsu, H. Sanada, H. Gotoh, T. Sogawa, H. Yamaguchi, *Vibration Amplification, Damping, and Self-Oscillations in Micromechanical Resonators Induced by Optomechanical Coupling through Carrier Excitation*, Phys. Rev. Lett. **106**, 036801 (2011).
- [14] S. Zaitsev, A. K. Pandey, O. Shtempluck, and E. Buks, *Forced and self-excited oscillations of an optomechanical cavity*, Phys. Rev. E **84**, 046605 (2011).
- [15] L. Zhang and H. Y. Kong, *Self-sustained oscillation and harmonic generation in optomechanical systems with quadratic couplings*, Phys. Rev. A **89**, 023847 (2014).
- [16] P. DelHaye, A. Schliesser, O. Arcizet, T. Wilken, R. Holzwarth and T. J. Kippenberg, *Optical frequency comb generation from a monolithic microresonator*, Nature **450**, 1214 (2007).
- [17] A. Jenkins, *Self-oscillation*, Phys. Rep. **525**, 167 (2013).
- [18] M. Gao, F. C. Lei, C. G. Du, and G. L. Long, *Self-sustained oscillation and dynamical multistability of optomechanical systems in the extremely-large-amplitude regime*, Phys. Rev. A **91**, 013833 (2015).
- [19] F. Marquardt, J. G. E. Harris, and S. M. Girvin, *Dynamical Multistability Induced by Radiation Pressure in High-Finesse Micromechanical Optical Cavities*, Phys. Rev. Lett. **96**, 103901 (2006).
- [20] T. Carmon, M. C. Cross, and Kerry J. Vahala, *Chaotic Quivering of Micron-Scaled On-Chip Resonators Excited by Centrifugal Optical Pressure*, Phys. Rev. Lett. **98**, 167203 (2007).
- [21] L. Bakemeier, A. Alvermann, and H. Fehske, *Route to Chaos in Optomechanics*, Phys. Rev. Lett. **114**, 013601 (2015).
- [22] Jonas Larson and Mats Horsdal *Photonic Josephson effect, phase transitions, and chaos in optomechanical systems*, Phys. Rev. A **84**, 021804(R) (2011).
- [23] X. Lü, H. Jing, J. Ma, and Y. Wu, *PT-Symmetry-Breaking Chaos in Optomechanics*, Phys. Re. Lett. **114**, 253601 (2015).
- [24] R. B. Karabalin, X. L. Feng, and M. L. Roukes, *Parametric Nanomechanical Amplification at Very High Frequency*, Nano Lett. **9**, 3116 (2009).
- [25] A. Nunnenkamp, K. Børkje, J. G. E. Harris and S. M.

- Girvin, *Cooling and squeezing via quadratic optomechanical coupling*, Phys. Rev. A **82**, 021806(R) (2010).
- [26] O. Arcizet, P.-F. Cohadon, T. Briant, M. Pinard and A. Heidmann, *Radiation-pressure cooling and optomechanical instability of a micromirror*, Nature **444** 71 (2006).
- [27] J. S. Aldridge and A. N. Cleland, *Noise-Enabled Precision Measurements of a Duffing Nanomechanical Resonator*, Phys. Rev. Lett. **94**, 156403 (2005).
- [28] I. Katz, A. Retzker, R. Straub, and R. Lifshitz, *Signatures for a Classical to Quantum Transition of a Driven Nonlinear Nanomechanical Resonator*, Phys. Rev. Lett. **99**, 040404 (2007).
- [29] Warner J. Venstra<sup>1</sup>, Hidde J. R. Westra, Herre S.J. van der Zant, *Stochastic switching of cantilever motion*, Nat. Comm. **4**, 2624 (2013).
- [30] I. Favero and K. Karrai, *Optomechanics of deformable optical cavities*, Nature Photonics **3**, 201 (2009).
- [31] D. Rugar, P. Grütter, *Mechanical parametric amplification and thermomechanical noise squeezing*, Phys. Rev. Lett. **67**, 699 (1991).
- [32] K. L. Turner, S. A. Miller, P. G. Hartwell, N. C. MacDonald, S. H. Strogatz, S. G. Adams, *Five parametric resonances in a micromechanical system*, Nature **396**, 149 (1998).
- [33] Junho Suh, M. D. LaHaye, P. M. Echternach, K. C. Schwab and M. L. Roukes, *Parametric Amplification and Back-Action Noise Squeezing by a Qubit-Coupled Nanoresonator* Nano Lett. **10**, 3990 (2010).
- [34] M. Ludwig, B. Kubala and F. Marquardt, *The optomechanical instability in the quantum regime*, New J. Phys. **10**, 095013 (2008).
- [35] L. Zhang and Z. Song, *Modification on static responses of a nano-oscillator by quadratic opto-mechanical couplings*, Sci. China Phys. Mech. Astron. **57**, 880 (2014).
- [36] I. Kozinsky, H. W. Ch. Postma, O. Kogan, A. Husain, and M.L. Roukes, *Basins of Attraction of a Nonlinear Nanomechanical Resonator*, Phys. Rev. Lett. **99**, 207201 (2007).
- [37] A. Dorsel, J. D. McCullen, P. Meystre, E. Vignes, and H. Walther, *Optical Bistability and Mirror Confinement Induced by Radiation Pressure*, Phys. Rev. Lett. **51**, 1550 (1983).
- [38] J. S. W. Lamb, and J. A. G. Roberts, *Time-reversal symmetry in dynamical systems: A survey*, Physica D **112**, 1 (1998).
- [39] M. Hossein-Zadeh and K. J. Vahala, *Observation of optical spring effect in a microtoroidal optomechanical resonator*, Opt. Lett. **32**, 1611 (2007).
- [40] B. S. Sheard, M. B. Gray, C. M. Mow-Lowry, D. E. McClelland and S. E. Whitcomb, *Observation and characterization of an optical spring*, Phys. Rev. A **69**, 051801(R) (2004).
- [41] A. Pikovsky, M. Rosenblum and J. Kurths, *Synchronization: a universal concept in nonlinear sciences*, Cambridge University Press, Cambridge UK (2001).
- [42] H. Seok, E. M. Wright, and P. Meystre, *Dynamic stabilization of an optomechanical oscillator*, Phys. Rev. A **90**, 043840 (2014).
- [43] G. J. Milburn, D. F. Walls, *Quantum nondemolition measurements via quadratic coupling*, Phys Rev A **28**, 2065 (1983).
- [44] M. R. Vanner, *Selective Linear or Quadratic Optomechanical Coupling via Measurement*, Phys. Re. X **1**, 021011 (2011).